Science Advances

AAAS

advances.sciencemag.org/cgi/content/full/2/6/e1600245/DC1

Supplementary Materials for

Role of scaffold network in controlling strain and functionalities of nanocomposite films

Aiping Chen, Jia-Mian Hu, Ping Lu, Tiannan Yang, Wenrui Zhang, Leigang Li, Towfiq Ahmed, Erik Enriquez, Marcus Weigand, Qing Su, Haiyan Wang, Jian-Xin Zhu, Judith L. MacManus-Driscoll, Long-Qing Chen, Dmitry Yarotski, Quanxi Jia

Published 10 June 2016, *Sci. Adv.* **2**, e1600245 (2016)
DOI: 10.1126/sciadv.1600245

The PDF file includes:

table S1. Vertical lattice strain reported in different systems with direct lattice matching. References can be found in the main text.

System	Bulk lattice constants (Å)	Lattice matching	Calculated lattice mismatch*	Strain from Experiments	Ref.
LCMO:MgO	3.86 : 4.21	1:1	8.67%	~2.1%	33
BFO:CFO	3.96 : 8.39	2:1	5.76%	1.0%	34
BTO:CFO	4.04 : 8.39	2:1	3.76%	1.6%	35
BFO:LSMO	3.96 : 3.87	1:1	2.29%	1.3%	20
YBCO:BZO	11.679 : 4.193	1:3	7.7%	1.0%	36
LSMO:MgO	3.87 : 4.21	1:1	8.41%	~2.0%	This work

*The calculated lattice mismatch is calcuated by using $200\%\times(a_1-a_2)/(a_1+a_2)$. a_1 and a_2 are the bulk lattice constant of these two components. It assumes that one of the phase is completely strained to another phase.

table S2. Vertical lattice strain reported in different systems with domain matching. It is the maximum strain one possibably can obtained in a system.

System*	Bulk lattice constants (Å)†	*m* value	Domain matching *m*:*m*+1	Calculated lattice mismatch	Strain from Experiments	Ref.
LSMO (001): ZnO (110)	3.87 : 3.24	5.14	5 : 6	0.46%	~0.5%, & 1.0%	12,17
LSMO (111): ZnO (0001)	6.703:5.213	3.50	7 : 9 (3:4+4:5)	8.5×10^{-3}%	0	14, 37
CeO_2:LSMO	5.411 : 3.87	2.51	5 : 7 (2:3+3:4)	0.13%	<0.1%	38
$SrZrO_3$:Er_2O_3	4.09 : 2.6375	1.82	2 : 3	3.32%	0.05%	39
$SrZrO_3$:Dy_2O_3	4.09 : 2.6675	1.88	2 : 3	2.19%	0.6%	39
$SrZrO_3$:Gd_2O_3	4.09 : 2.7	1.94	2 : 3	0.98%	0.9%	39
$SrZrO_3$:Eu_2O_3	4.09 : 2.7125	1.97	2 : 3	0.52%	1.1%	39
$SrZrO_3$:Sm_2O_3	4.09 : 2.73	2.01	2 : 3	0.12%	1.3%	39
BTO:Sm_2O_3	4.04 : 2.73	2.08	2 : 3	1.17%	2.35%	27
BFO:Sm_2O_3	3.96 : 2.73	2.22	7 : 10 (2:3+2:3+3:4)	1.71%	~1.4%	12
STO:Sm_2O_3	3.905 : 2.73	2.32	7 : 10 (2:3+2:3+3:4)	0.31%	--	24

*The calculated *m* value is 3.51 for CeO_2:LSMO, therefore, *m* can be valued as 3 or 4, in this case. Therefore, both 2:3 and 3:4 matchings exist. In the $SrZrO_3$:RE_2O_3 systems, the calculated *m* values range from 1.82 to 2.01, therefore, the *m* is set to 2 for domain matching. It should be noted that the calculated misfit strain in the out-of-plane is very different from Ref. 39. In previous reports, we can find that both the RE_2O_3 phase (e.g. Sm_2O_3) and active phase (e.g. $SrZrO_3$, BTO) are (00*l*) oriented along out-of-plane. Therefore, the out-of-plane strain should be calculated between (00*l*) planes rather than between (00*l*) planes and (0*ll*) planes.

†Bulk lattice constant of Er_2O_3 is 10.55 Å. The plane Er_2O_3 (004) spacing is 10.55 Å /4=2.6375 Å. Bulk lattice constant of Dy_2O_3 is 10.67 Å. The plane Dy_2O_3 (004) spacing is 10.67 Å /4=2.6675 Å. Bulk lattice constant of Gd_2O_3 is 10.80 Å. The plane Gd_2O_3 (004) spacing is 10. 80 Å /4=2.7 Å. Bulk lattice constant of Eu_2O_3 is 10.85 Å. The plane Eu_2O_3 (004) spacing is 10. 85 Å /4=2.7125 Å. Bulk lattice constant of Sm_2O_3 is 10.92 Å. The plane Sm_2O_3 (004) spacing is 10.92 Å /4=2.73 Å. The bulk lattice parameters of these five RE_2O_3 materials are adopted from Ref. 39.

table S3. The lattice parameter of LSMO:MgO nanoscaffolding films.

System	a_{ip} (Å)	a_{oop} (Å)	ε_{ip}*	ε_{oop}	K_{me} (erg/cm^3)†	Unit cell volume‡
LSMO:MgO (0%)	3.886	3.852	0.90%	-0.45%	-6.56×10^5	58.169
LSMO:MgO (5%)	3.879	3.867	0.38%	-0.0775%	-0.11×10^5	58.185
LSMO:MgO (11%)	3.870	3.886	0%	0.42%	6.13×10^5	58.200
LSMO:MgO (15%)	3.865	3.896	-0.15%	0.67%	9.78×10^5	58.199
LSMO:MgO (22%)	3.858	3.924	-0.31%	1.39%	20.3×10^5	58.405
LSMO:MgO (40%)	3.851	3.938	-0.49%	1.76%	25.7×10^5	58.401

*The out-of-plane and in-plane lattice mismatch (a_{oop} and a_{ip}) of the LSMO phase in the nanocomposite can be expressed as $\varepsilon_{oop}=(a_{oop}-a_{bulk})/a_{bulk}$ and $\varepsilon_{ip}=(a_{ip}-a_{bulk})/a_{bulk}$, where a_{bulk} of LSMO is 3.87Å.

†The demagnetization energy $2\pi M^2$ is determined to be 3.93×10^5 erg/cm^3, considering the saturated magnetization M is 226 emu/cc (15% MgO). Magnetoelastic anisotropy energy along [001] direction.

‡Unit cell volume of unstrained LSMO is 57.96 Å.

table S4. The elastic stiffness tensor of the materials used in our work.

Materials	C_{11} (GPa)	C_{12} (GPa)	C_{44} (GPa)	*Ref*	Lattice mismatch *
MgO	293	92	155	54	8.41% (see table S1)
ZnO	209	C_{12}=104.6	C_{33}=210.6 C_{55}=42.3 C_{66}=44.3	56	0.46% (see table S2)
LSMO†	227.2	158.6	66.5	46	
$SrTiO_3$	318	102	123	55	

*The lattice mismatch is calculated between LSMO and MgO, and between LSMO and ZnO.

†The elastic modulus of LSMO is adopted from a $La_{0.83}Sr_{0.17}MnO_3$ single crystal.

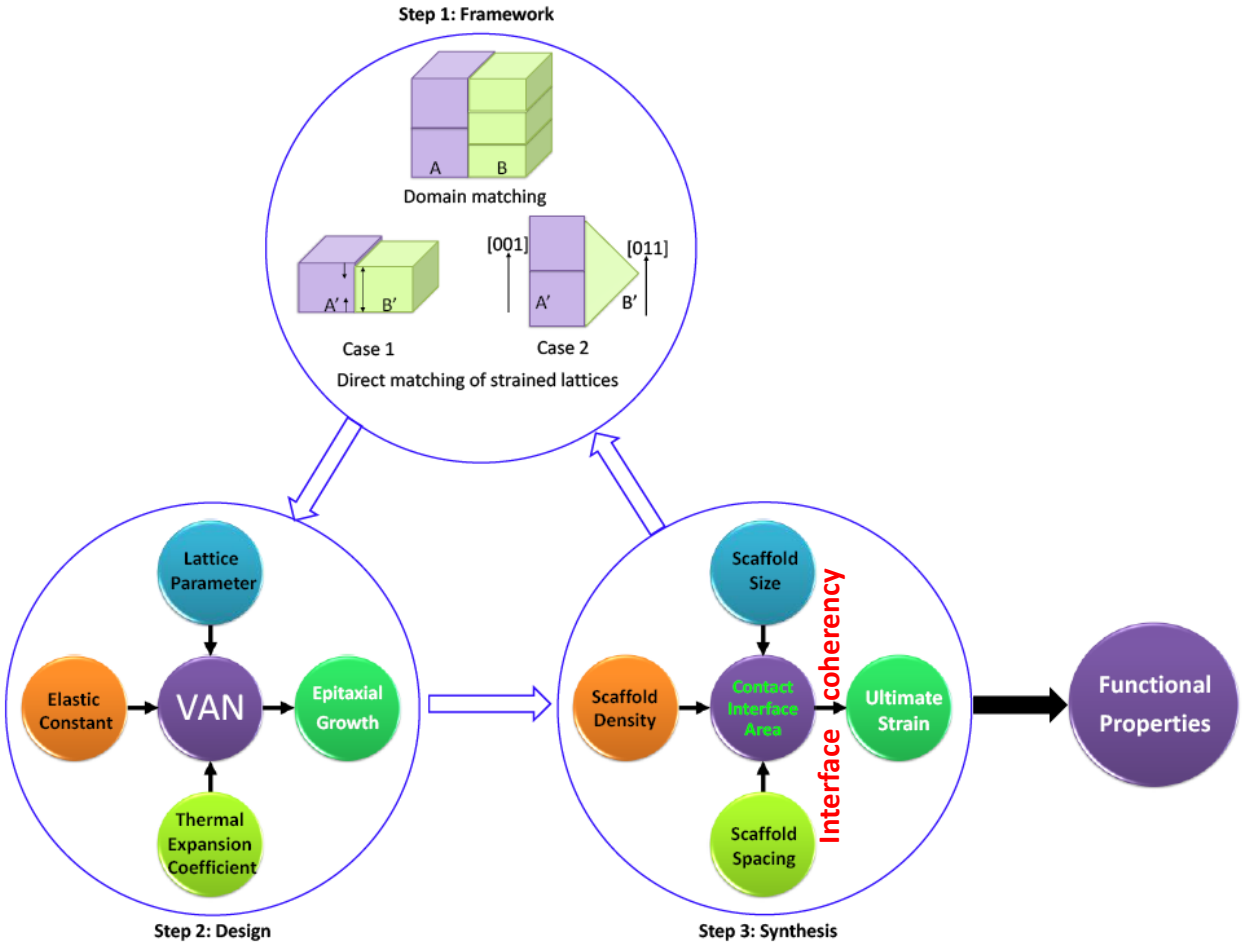

fig. S1. Strain design flow in vertical nanocomposites. Step 1 is the framework of the domain matching along the vertical interface. It shows two lattices of "A" match with three lattices of "B". Schematic illustration of direct matching of strain lattices with 1:1 matching. In some cases, two lattices A' match with one lattice B' along the [011] direction. Step 2 is the design of two components. There are quite a few critical factors in determining the strain of nanocomposites during the design stage. Step 3 is the synthesis of nanocomposite films. During the synthesis stage, the vertical interface contact area and the misfit dislocations at vertical interface are the ultimate parameters to control the vertical strain.

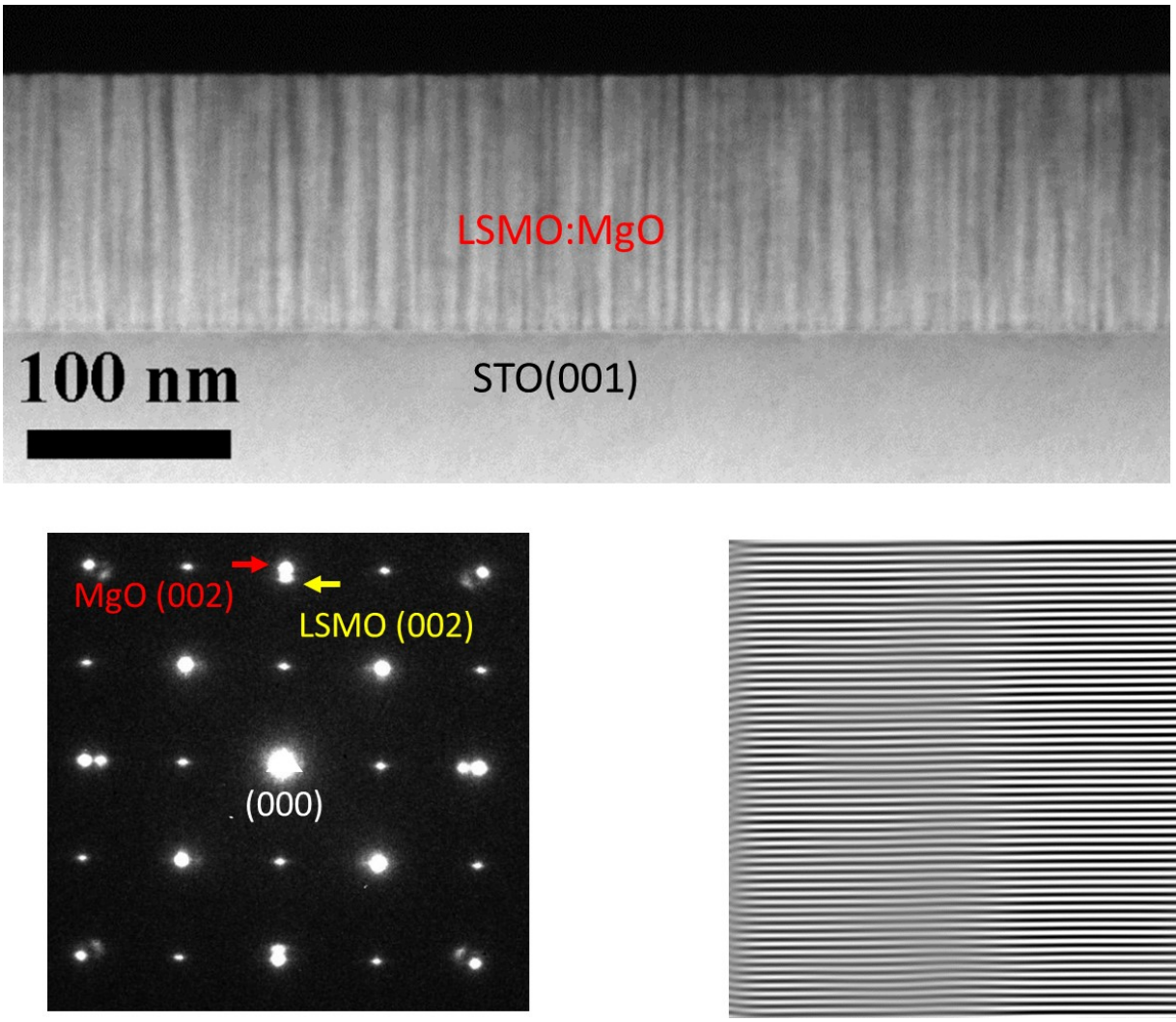

fig. S2. Microstructure of LSMO:MgO nanoscaffolding films. Low magnefication cross-sectional STEM image showing the alternating growth of LSMO (white) and MgO vertical nanowires (dark) on STO (001) substrates. The selected area electron diffraction of the LSMO:MgO film. Only the nanoscaffolding film was included in the diffraction pattern. The FFT image is corresponding with Fig. 1D in the manuscript. The reasons we select MgO as the secondary phase are because (1) MgO has a cubic structure with a lattice constant of 4.21Å, which has a large lattice mismatch of 8.41% with the LSMO phase; (2) MgO is stable at growth temperature and can be epitaxially grown on STO with the LSMO phase; (3) Mg has very different Z number with La, which gives good contrast for STEM characterizations.

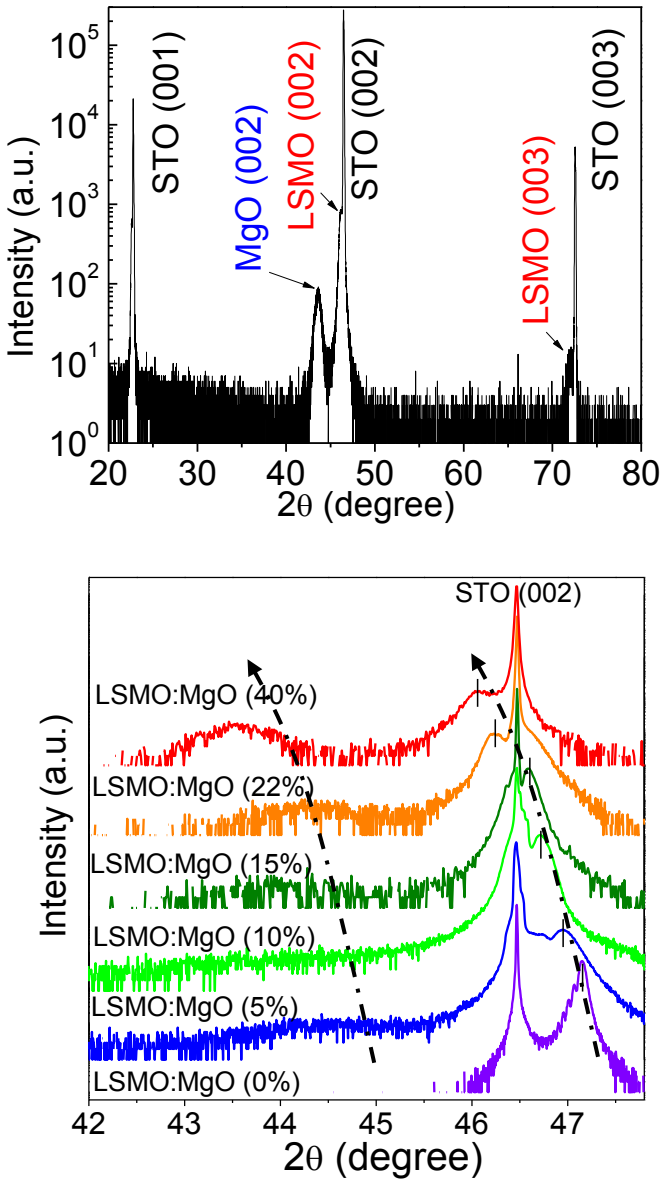

fig. S3. **XRD of LSMO:MgO nanoscaffolding films.** XRD scan of 450 nm LSMO:MgO (40%) nanoscaffolding films. Local XRD scan of LSMO:MgO with different MgO volumes. The dash curve guide the shift of LSMO (002) and MgO (002) peaks from right to left. It indicates the out-of-plan lattice parameters of both the LSMO and MgO phases increase with increasing the MgO volume.

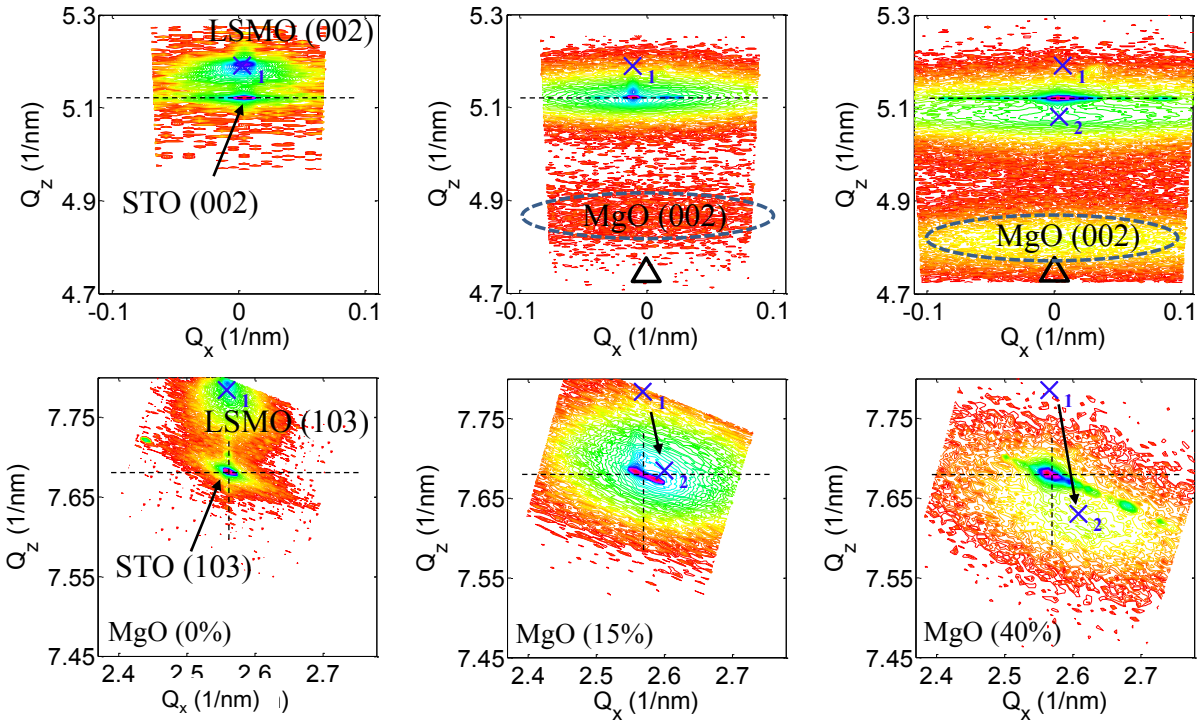

fig. S4. **RSM of LSMO:MgO nanoscaffolding films.** RSM (002) of pure LSMO, LSMO:MgO with 15 % MgO, and LSMO:MgO with 40 % MgO. RSM (103) of pure LSMO, LSMO:MgO with 15 % MgO, and LSMO:MgO with 40 % MgO. The "X_1" and "Δ" represent the position of single phase LSMO and MgO films, respectively. The "X_2"represents the position of LSMO peak after inserting MgO nanoscaffolds.

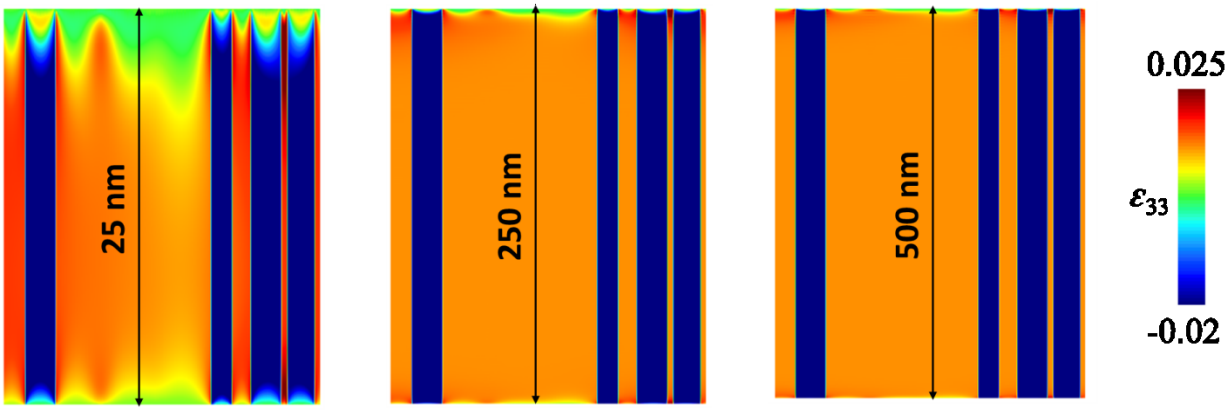

fig. S5. **Strain distribution in LSMO:MgO nanoscaffolding films.** Calculated strain distribution in LSMO matrix and MgO nanoscaffolds of 25 nm, 250 nm and 500 nm thin films. The MgO volume ratio is ~23%.

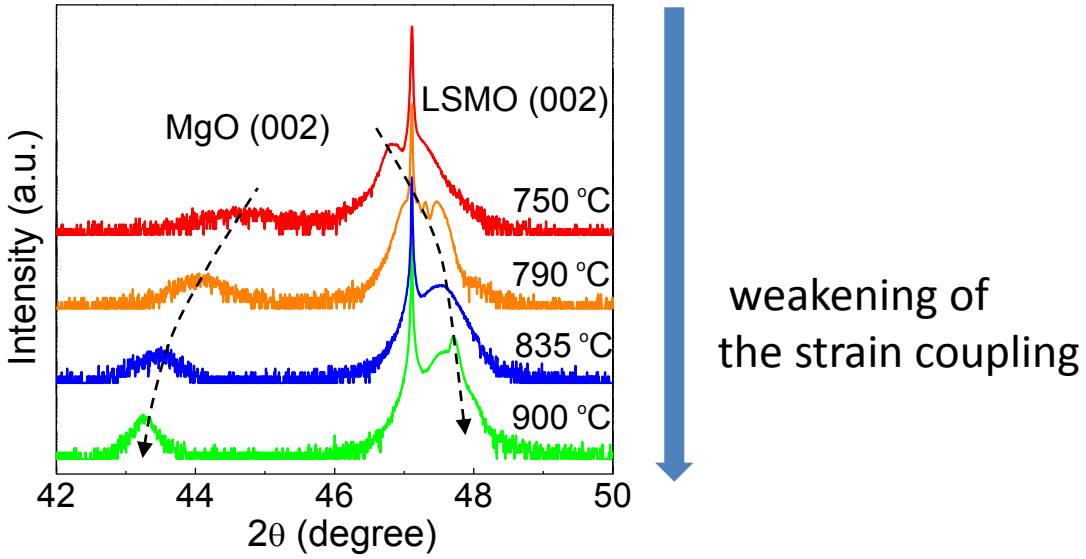

fig. S6. **XRD of LSMO:MgO nanoscaffolding films deposited at different temperatures.** Temperature dependent MgO and LSMO peak shift in 600 nm LSMO:MgO nanocomposite thin films.

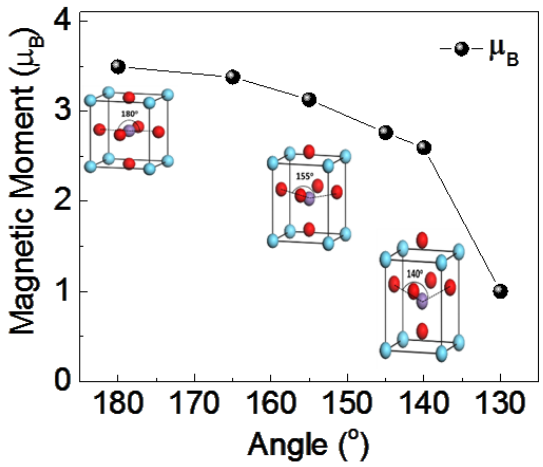

fig. S7. **Strain dependent magnetic properties**. Net magnetic moment on Mn ion as function of O-Mn-O angle in 'xy' plane. Inset represents three different unit cells with increasing '*c/a*' ratio which reflect increased strain on them due to increasing MgO volume ratio. Each case also has a corresponding oxygen distortion namely 180º, 155º, and 140º.

In order to have a theoretical understanding of our experimental results, we performed first-principles investigation of magnetization in $LaMnO_3$ (LMO) bulk and its dependence on strain induced oxygen distortion. Our density functional theory (DFT) calculations show an overall reduction of the net magnetic moment in LMO. Such reduction is caused by interfacial strain, induced by MgO nanowires. Strain on LMO near the interface increases with higher volume ratio of LMO:MgO. Earlier works (*7*) have demonstrated distortion of oxygen octahedron in the perovskite unit cells under strain. In $LaMnO_3$, the magnetization is dominantly contributed by the Mn cation. The O-Mn bond distance plays an important role in controlling the charge transfer from O to Mn ions, and thus dictates the final net magnetic moment. To explain the interplay between the O-Mn distance and final magnetic moment on Mn ion, we have taken a simple model approach. In this proof of principles calculation, we have considered different O-Mn-O angles by vertically shifting the oxygen octahedron. Each of these angular configurations (fig. S7) is associated with unit a cell with different *c/a* ratios. Increasing values for *c/a* indicate higher strain on LMO caused by increasing volume ratio of MgO pillars in LMO matrix. Thus, a positive correlation is assumed between the MgO pillar volume ratio and O-Mn-O distortion angle in this simple model. For different O-Mn-O distortion angles, we have performed DFT calculations where magnetic moment on Mn ion is self-consistently determined. We observe an

overall decrease of magnetic moment (fig. S7) with smaller O-Mn-O angles which are associated with larger MgO volume ratio, and therefore, larger strain. This is consistent with our experimental findings in Fig. 3E. The strain induced lattice distortion and octahedral rotation changes the Mn-O-Mn angle and distance, which reduces the magnetism. Under an extreme large strain, the conduction carriers are fully localized. Thus, significantly resistance rise and magnetization drop are observed (*9*). We have used Full potential LAPW based density functional theory code as implemented in Wien2K. For exchange-correlation functional, we used PBE (*49*). The Brillouin zone is sampled with 8x8x7 k points. For lattice constants we have used experimental values for each of the MgO volume ratio case and correspondingly selected a larger angular distortion with smaller O-Mn-O angle.

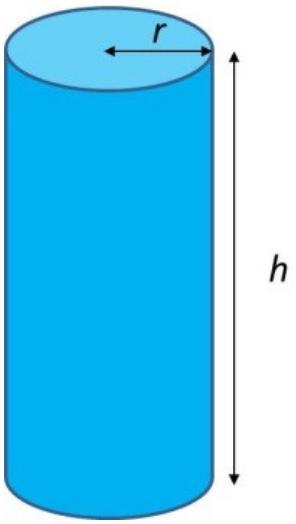

fig. S8. The relationship between pillar surface area and volume with fixed radius. The schematic illustration of the MgO cylinder in LSMO matrix. Assume there are m of MgO cylinders, with a radius of r and a height of h. The total volume of MgO cylinders is V. Therefore, $V=m\times\pi r^2\times h$. The total surface area (S) of m MgO cylinders is given by, $S=m\times 2\pi r\times h=2\pi r\times V/(\pi r^2)=2V/r$. The nanoscaffold MgO surface area S is linearly proportional to its volume V if the dimension of the scaffolds size is constant. When V is fixed, S is inversely proportional to the radius r.

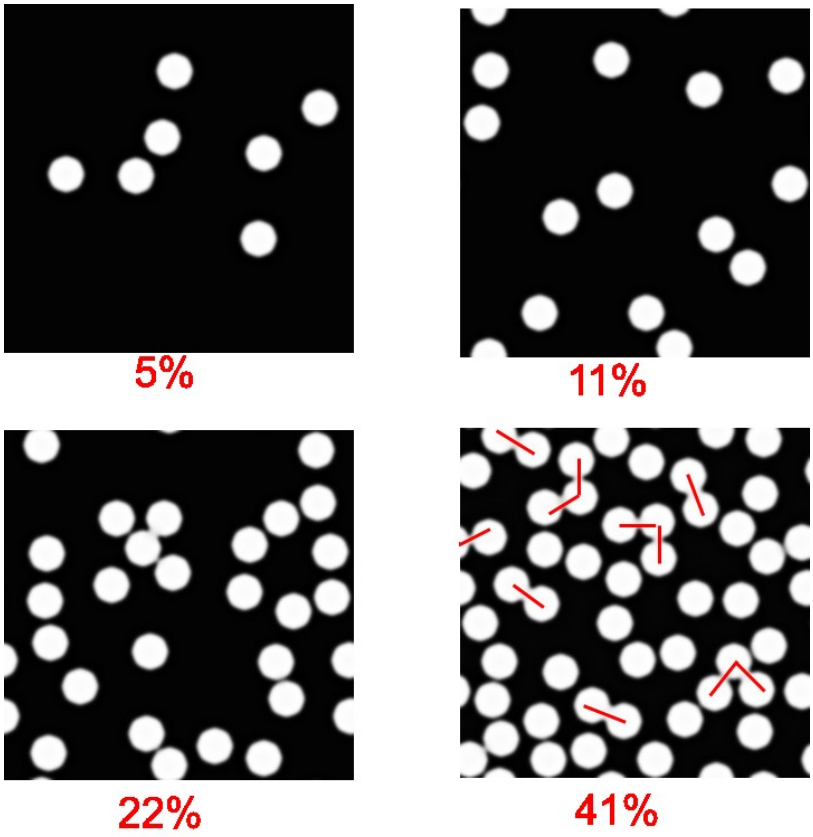

fig. S9. The simulated microstructure of nanoscaffolding films. Simulation of nanoscaffolds distribution in a matrix with MgO volume of 5%, 11%, 22 % and 41%.The red lines represent the contact of nanoscaffolds, reducing the total scaffold vertical area.

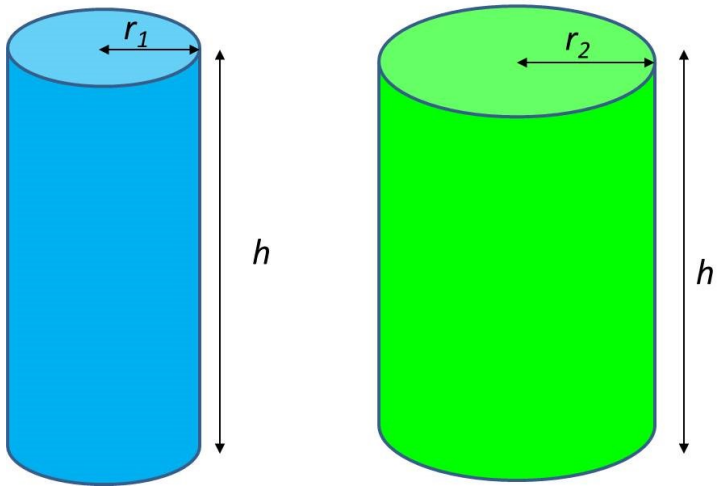

fig. S10. the relationship between pillar surface area and radius with fixed volume. The schematic illustration of the MgO cylinder in LSMO matrix with different sizes (r_1 and r_2), but the MgO volume is fixed. Assume there are m of MgO cylinders, when the radius of MgO is r_1 and the height is h. Assume there are n of MgO cylinders, when the radius of MgO is r_2 and the height is h. The total volume of MgO cylinders, V, is fixed. Therefore, $V=m\times\pi r_1^2\times h= n\times\pi r_2^2\times h$. The total surface area (S_1) of m MgO cylinders is given by, $S_1=m\times 2\pi r_1\times h$; and the total surface area (S_2) of n MgO cylinders is given by, $S_2=m\times 2\pi r_2\times h$. Therefore, $S_1 / S_2 = r_2 / r_1$. This is also consistent with the discussion in fig. S8 that the nanoscaffold MgO surface area S is inversely proportional to its radius r when the V is fixed.

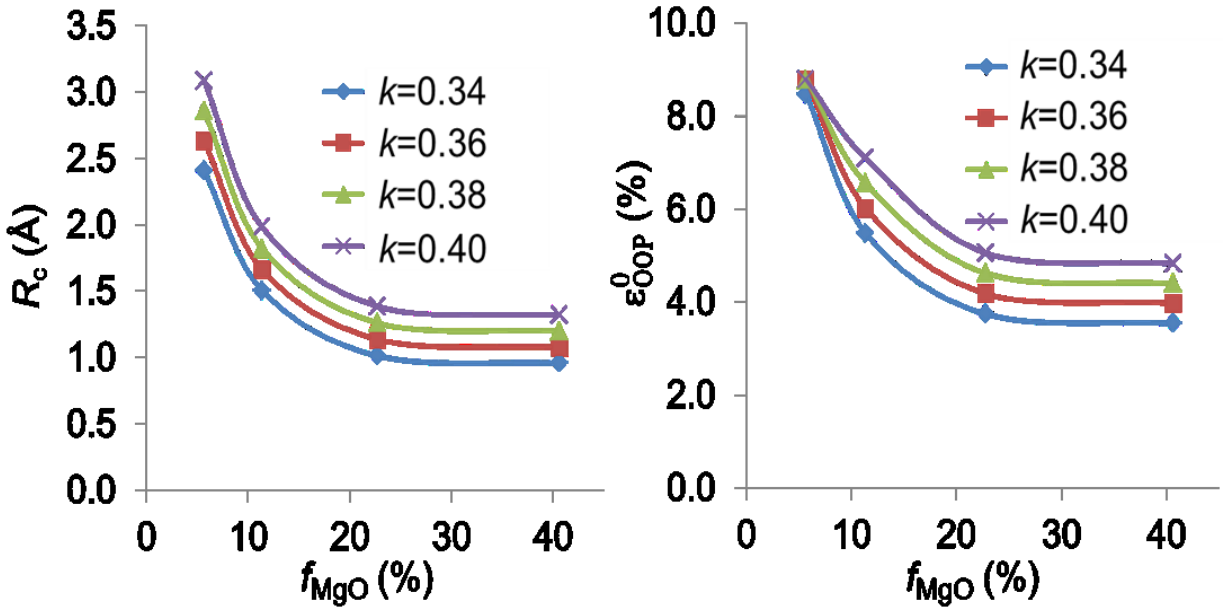

fig. S11. Critical radius (R_c) and the residual vertical mismatch strain (ε^0_{OOP}) of the MgO pillar as a function of the volume ratio of the MgO pillars (f_{MgO}).

S1. Deriving the analytical expressions of critical thickness (h_c) and radius (R_c) in vertical nanocomposite thin films

1. Deriving h_c

The expression of h_c is derived following conventional epitaxial theory. As mentioned in main text, the area elastic energy density (f_{elast}) equals the area energy cost of forming an interfacial dislocation (f_{disl}). For cubic MgO, f_{elast} is expressed as (*58*)

$$f_{\text{elast}}(h) = 2\text{G}h\frac{1+v}{1-v}\left(\varepsilon_{app}\right)^2 \tag{S1}$$

The energy per unit length (J/m) of an edge dislocation, $f^{\text{L}}_{\text{disl}}$ can be written as (*59*)

$$f^{\text{L}}_{\text{disl}}(h) = \frac{Gb^2\left(1-v\cos^2\beta\right)}{4\pi(1-\text{v})}\ln\frac{\alpha h}{b} \tag{S2}$$

where β is the angle between the Burger's vector and dislocation line (=90◦ for a Burger's vector of pure edge character), and α is the cut-off parameter describing the energy of the dislocation core (taken as 1 herein). Given that the density of interfacial dislocations ρ (m^{-1}) can be approximated as $\rho \approx \varepsilon_{app}/b$, the area formation energy of dislocation f_{disl} can be expressed as

$$f_{\mathrm{disl}}(h) = \rho f_{\mathrm{disl}}^{\mathrm{L}} = \frac{Gb\varepsilon_{\mathrm{app}}}{4\pi(1-\nu)} \ln \frac{h}{b} \tag{S3}$$

Equation 3 in the main text can therefore be obtained by considering $f_{elast}(h_c)=f_{disl}(h_c)$

2. Deriving R_c

To derive the analytical expression of the critical MgO pillar radius (R_c) for the formation of dislocations at the vertical LSMO-MgO interface, corresponding analytical expressions of the elastic energy density cost (f_{elast}) and dislocation energy density (f_{disl}) must be known.

The elastic energy density cost (f_{elast}) for such vertical LSMO-MgO nanocomposite film can be written as

$$f_{elast} = \left(1 - f_{\mathrm{MgO}}\right) \frac{1}{2} s_{33}^{\mathrm{LSMO}} \left(\sigma_{33}^{\mathrm{LSMO}}\right)^2 + f_{\mathrm{MgO}} \frac{1}{2} s_{33}^{\mathrm{MgO}} \left(\sigma_{33}^{\mathrm{MgO}}\right)^2 \tag{S4}$$

where the elastic compliance coefficient $s_{33}=s_{11}=1/Y$ for cubic symmetry; the out-of-plane stresses can be expanded as

$$\sigma_{33}^{\mathrm{q}} = 2c_{12}^{\mathrm{q}}\left(\varepsilon_{11}^{\mathrm{q}} - \varepsilon^{0-\mathrm{q}}\right) + c_{11}^{\mathrm{q}}\left(\varepsilon_{33}^{\mathrm{q}} - \varepsilon^{0-\mathrm{q}}\right), \mathrm{q} = \mathrm{LSMO}, \mathrm{MgO} \tag{S5}$$

where the eigenstrain $\varepsilon^{0-\mathrm{q}}$ is induced from lattice mismatch between the phases, and is zero for q=LSMO because LSMO is taken as the reference. Thus the only unknown parameters in eq. S5 are the in-plane and out-of-plane total strains $\varepsilon_{11}^{\mathrm{q}}$ and $\varepsilon_{33}^{\mathrm{q}}$, which can be obtained by considering the following mechanical boundary conditions of a vertical nanocomposite thin film

$$\left(1-f_{\mathrm{MgO}}\right)\left(\varepsilon_{11}^{\mathrm{LSMO}}\right)+f_{\mathrm{MgO}}\left(\varepsilon_{11}^{\mathrm{MgO}}\right)=\varepsilon^{0-\mathrm{STO}} \quad \text{(S6a)}$$

$$\sigma_{11}^{\mathrm{LSMO}}=\sigma_{11}^{\mathrm{MgO}},\varepsilon_{33}^{\mathrm{LSMO}}=\varepsilon_{33}^{\mathrm{MgO}}=\varepsilon_{33} \quad \text{(S6b)}$$

$$\left(1-f_{\mathrm{MgO}}\right)\left(\sigma_{33}^{\mathrm{LSMO}}\right)+f_{\mathrm{MgO}}\left(\sigma_{33}^{\mathrm{MgO}}\right)=0 \quad \text{(S6c)}$$

Where the eigenstrain $[\varepsilon^{0-\mathrm{STO}}=(a_{\mathrm{STO}}-a_{\mathrm{LSMO}})/a_{\mathrm{LSMO}}]$ arises from the lattice mismatch between STO and the reference LSMO phase. For simplicity, the same elastic modulus is utilized for LSMO and MgO phases. A combination of eqs. S4-S6 yields the expression for f_{elast}, expressed as

$$f_{\mathrm{elast}}=\frac{1}{2}\left(1-f_{\mathrm{MgO}}\right)f_{\mathrm{MgO}}Y\left(\varepsilon^{0-\mathrm{MgO}}\right)^2 \quad \text{(S7)}$$

where the eigenstrain $\varepsilon^{0-\mathrm{MgO}}=\left(a_{\mathrm{MgO}}-a_{\mathrm{LSMO}}\right)/a_{\mathrm{LSMO}}$ describes the lattice mismatch between MgO and LSMO.

Now turn to deriving the dislocation energy density (f_{disl}) at the LSMO-MgO interface. First, the expression of the energy per unit length (J/m) of an edge dislocation, $f_{\mathrm{disl}}^{\mathrm{L}}$ can be written similarly to eq. S2

$$f_{\mathrm{disl}}^{\mathrm{L}}(R)=\frac{Gb^2}{4\pi(1-\mathrm{v})}\ln\frac{2R}{b} \quad \text{(S8)}$$

where R is the radius of the MgO pillar. Let us assume the edge dislocations at the vertical interface form closed dislocation loops, which has a radius of r and encompasses more than one MgO pillars. Then it is rational to assume $= kR\sqrt{f_{\mathrm{MgO}}}$, where k (k>0) is a pre-factor fitted from experimental data. Here we name one group of MgO pillars, which are encompassed by N dislocation loops, as one dislocation site. The areal density of these dislocation sites (ρ_0, in the unit of m^{-2}) can be estimated as $\rho_0=1/k^2\pi R^2$. In addition, the number of dislocation loops (N) per dislocation site can be estimated as $N=h\varepsilon_{\mathrm{app}}/b$, with $\varepsilon_{\mathrm{app}}=\varepsilon^{0-\mathrm{MgO}}$ and h representing the film thickness. Building on these the areal energy density of dislocations in the nanocomposite (f_{A}, in the unite of J/m^2) can be calculated as

$$f_{\mathrm{A}} = \rho_0 \cdot N \cdot 2\pi r \cdot f_{\mathrm{disl}}^{\mathrm{L}} = \frac{2h\varepsilon_{\mathrm{app}}\sqrt{f_{\mathrm{MgO}}}}{kbR} f_{\mathrm{disl}}^{\mathrm{L}} \quad \text{(S9)}$$

The volumetric dislocation energy density (f_{disl}) can then be obtained by dividing f_{A} with the thickness h, i.e.

$$f_{\mathrm{disl}}(R) = \frac{2\varepsilon_{\mathrm{app}}\sqrt{f_{\mathrm{MgO}}}}{kbR} f_{\mathrm{disl}}^{\mathrm{L}}. \quad \text{(S10)}$$

Equation 4 in the main text can therefore be obtained by considering $f_{\mathrm{disl}}(R_{\mathrm{c}})=f_{\mathrm{elast}}$ (see eq. S7). As shown in fig. S11, the calculated critical radius (R_{c}) and the resultant residual vertical mismatch strain $\varepsilon_{\mathrm{OOP}}^{0}$ (see main text) decrease nonlinearly with the increasing volume fraction of MgO pillars (f_{MgO}). This is a result of the nonlinearly increased density of interfacial dislocations.